Two-dimensional Chern semimetals on the Lieb lattice

Giandomenico Palumbo and Konstantinos Meichanetzidis
School of Physics and Astronomy, University of Leeds, Leeds, LS2 9JT, United Kingdom
(Received 11 July 2015; revised manuscript received 11 November 2015; published 4 December 2015)

In this work we propose a simple model that supports Chern semimetals. These gapless topological phases share several properties with the Chern insulators like a well-defined Chern number associated with each band, topologically protected edge states and topological phase transitions that occur when the bands touch each, with linear dispersion around the contact points. The tight-binding model, defined on the Lieb lattice with intra-unit-cell and suitable nearest-neighbor hopping terms between three different species of spinless fermions, supports a single Dirac-like point. The dispersion relation around this point is fully relativistic and the 3×3 matrices in the corresponding effective Hamiltonian satisfy the Duffin-Kemmer-Petiau algebra. We show the robustness of the topologically protected edge states by employing the entanglement spectrum. Moreover, we prove that the Chern number of the lowest band is robust with respect to weak disorder. For its simplicity, our model can be naturally implemented in real physical systems like cold atoms in optical lattices.

DOI: 10.1103/PhysRevB.92.235106 PACS number(s): 71.10.Pm, 03.65.Vf, 71.10.Fd, 71.20.Gj

I. INTRODUCTION

Topological phases represent one of the most exciting and interesting fields of condensed matter physics. Topological insulators and superconductors are well-known examples of free-fermion systems defined by a gapped bulk that supports robust gapless edge states [1]. All these systems described by noninteracting Hamiltonians fit in the periodic table of fermionic topological phases and the topological phase transitions occur when the bulk gap closes. In particular, two-dimensional chiral topological systems like the Haldane model [2] and p-wave superconductors [3] are characterized by the topological Chern number that fixes the number of topologically protected edge modes. The former is an example of a topological insulator in class A, called also Chern insulator, where both time-reversal and particle-hole symmetries are broken while the latter is a topological superconductor living in class D, where particle-hole symmetry is instead preserved.

In the last few years, part of the research of new topological phases has focused on gapless bulk systems like three-dimensional Weyl [4] and Dirac semimetals [5] that represent three-dimensional versions of graphene. In these systems, the bands touch each other in a discrete set of points that can be seen as pointlike defects in momentum space. These Weyl and Dirac points are topologically protected by well-defined Berry phases and the boundaries support suitable gapless modes. Clearly, when the time-reversal symmetry is broken in two dimensions, the Chern number can characterize the bands of the semimetals only when those bands do not touch each other, i.e., when there are no Dirac or Weyl cones. Some extended Haldane models with these characteristics have recently been analyzed [6,7].

The goal of this work is to present a simple model that supports two-dimensional Chern semimetallic phases, which share several properties with the Chern insulators. Our tight-binding model is defined on a Lieb lattice with intra-unit-cell and suitable nearest-neighbor hopping terms between three species of free spinless fermions. The model supports only a Dirac-like cone due to the presence of a zero-energy flat band in the middle. In fact, it is possible to avoid the fermion doubling in the lattice if a flat band is present. At this point, it is possible to deform the bands by introducing a further hopping term between nonadjacent fermions in the unit cell. In this case, as we show in the next section, the lower band is characterized by a nonzero Chern number $\nu = \pm 1$ and the model supports robust edge states. We analyze the edge modes by employing the entanglement spectrum and we demonstrate the robustness of the Chern number with respect to the presence of weak disorder. Moreover, we show that the corresponding effective Hamiltonian h_{eff} is fully relativistic but different with respect to a Dirac Hamiltonian, because the 3×3 matrices in h_{eff} satisfy the Duffin-Kemmer-Petiau algebra [8]. This implies that our model does not fit in any already known periodic table of topological gapless phases based on K theory and Clifford algebra [9]. Finally, due to the presence of only intra-unit-cell and suitable nearest-neighbor hopping terms, our model can be easily implemented in real physical systems like cold atoms in optical lattices.

II. LATTICE MODEL AND CHERN NUMBER

To begin with, we introduce our tight-binding model. We consider three species of spinless fermions on a Lieb lattice as shown in Fig. 1, described by the following Hamiltonian:

$$H = \sum_{\boldsymbol{i}} [J(a_{\boldsymbol{i}}^{\dagger} b_{\boldsymbol{i}} + b_{\boldsymbol{i}}^{\dagger} c_{\boldsymbol{i}}) + K(a_{\boldsymbol{i}}^{\dagger} b_{\boldsymbol{i}+\hat{x}} + b_{\boldsymbol{i}}^{\dagger} c_{\boldsymbol{i}+\hat{y}}) + M c_{\boldsymbol{i}}^{\dagger} a_{\boldsymbol{i}}] + \text{H.c.}, \tag{1}$$

where i is the site index, $\hat{x} = (1,0)$, $\hat{y} = (0,1)$, and a, b, and c are the three species of fermions represented in Fig. 1 in terms of triangles, circles, and squares, respectively. Here the tunneling coefficients J and K are taken real, while $M = m\, e^{i\theta}$ is complex. By imposing periodic boundary conditions we introduce the Fourier transformation $a_{k,\boldsymbol{i}} = \sum_{\boldsymbol{p}} e^{i\boldsymbol{p}\cdot\boldsymbol{i}} a_{k,\boldsymbol{p}}$, where $k = 1,2,3$ is the species index, to obtain $H = \sum_{\boldsymbol{p}} \psi_{\boldsymbol{p}}^{\dagger} h(\boldsymbol{p}) \psi_{\boldsymbol{p}}$, where $\psi_{\boldsymbol{p}} = (a_{\boldsymbol{p}}, b_{\boldsymbol{p}}, c_{\boldsymbol{p}})^T$, $\boldsymbol{p} \in \text{BZ} = [-\pi,\pi) \times [-\pi,\pi)$, and the kernel $h(\boldsymbol{p})$ is a 3×3 Hermitian matrix. It is straightforward to see that the time-reversal symmetry is broken, namely

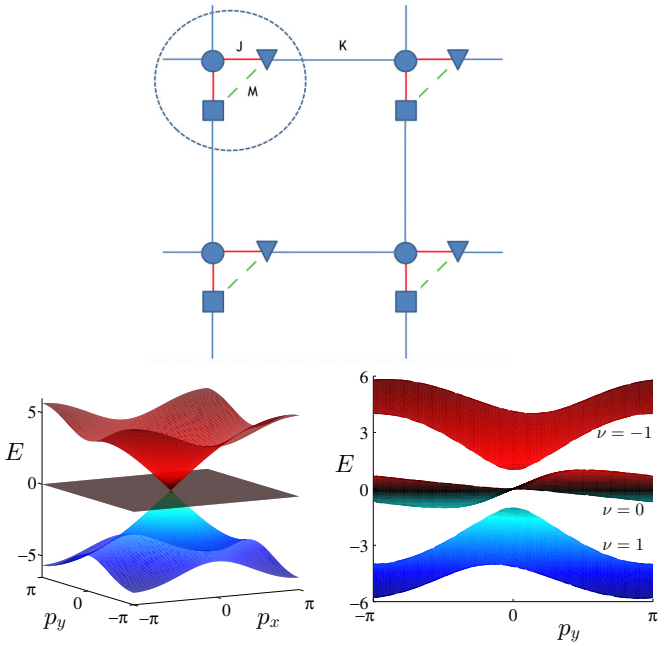

FIG. 1. (Color online) (Top) This picture shows a square lattice with three species of fermions represented by triangles, circles, and squares. The dashed circle encloses the unit cell. Intra-unit-cell hopping terms are represented by red lines and the nearest-neighbor ones with blue lines. The dashed green line identifies the hopping between nonadjacent fermions. (Bottom left) Dispersion energy for $K = -J = 1$ and $M = 0$. (Bottom right) Projection of dispersion energy for $M = 0.5i$.

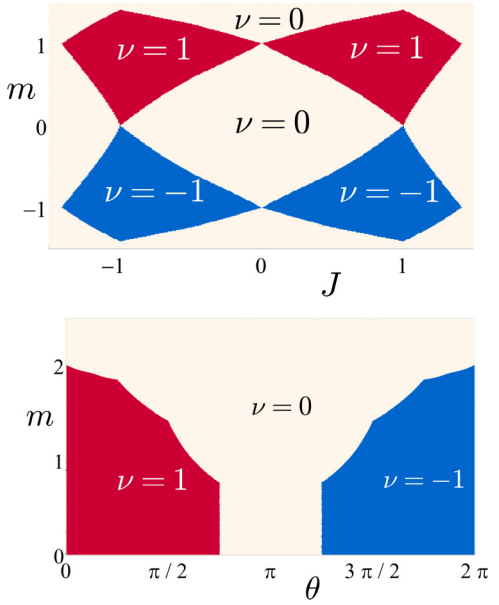

FIG. 2. (Color online) (Top) Chern number phase diagram in function of J and m with $K = 1$ and $\theta = \pi/2$ when the lowest band is completely filled. (Bottom) Phase diagram in function of m and θ with $K = -J = 1$.

$h(\boldsymbol{p}) \neq h^*(-\boldsymbol{p})$, but is restored when M is real. In particular, when $M = 0$, the system supports a single Dirac-like cone and a zero-energy flat band as shown in Fig. 1. First of all, the presence of the flat band allows us to avoid the fermion doubling problem as shown in [10]. In this case, our model behaves similarly to other three-band models defined on Lieb and Kagome lattices [11–16]. However, a crucial difference emerges with respect to the latter, when a nonzero complex M is switched on. In this case, the complex hopping term with a small $m < 1$ opens an indirect gap of value zero between the lower and upper bands and deforms the middle bands such that the systems remains gapless as shown in Fig. 1. Interestingly, the vanishing band gap associated with the topological gapless phases is firm for a large set of values of parameters in (1). A three-band Chern insulator can be built on the lattice only by adding suitable next-nearest-neighbor hoppings. We now show that in the semimetallic phase, our model behaves as a nontrivial topological semimetal, where each band has a well-defined Chern number ν. This is indeed possible because the time-reversal symmetry is broken and the bands do not touch each other at any point in the BZ like for example in graphene and Weyl semimetals. The Chern number related to the nth band with normalized Bloch wave function $|n(\boldsymbol{p})\rangle$ is defined by

$$\nu_n = \frac{1}{2\pi\, i} \int_{\mathrm{BZ}} d^2 p\, F_{xy}, \tag{2}$$

where the Berry connection A_α ($\alpha = x, y$) and the corresponding curvature tensor F_{xy} are given by $A_\alpha = \langle n(\boldsymbol{p})| \frac{\partial}{\partial p_\alpha} |n(\boldsymbol{p})\rangle$ and $F_{xy} = \partial_x A_y - \partial_y A_x$. Here we are assuming that there is no degeneracy for the nth state and we obtain a Chern number $\nu = \pm 1$ by integrating the Berry curvature on the lower band. For our numerical calculations, we use the discretized version of (2) derived in [17]. From a geometric point of view, the presence of the Chern number is connected to the presence of a nonzero flux passing through the triangles defined by the hoppings J and M inside the unit cell when M is complex. Figure 2 reproduces the phase diagram of this topological phase for $K = 1$ and $\theta = \pi/2$ and displays how the chirality depends on the sign of m and J. Importantly, topological phase transitions occur when the bands touch each other, with linear dispersion around the contact points. Moreover, as we show in the next section, topologically edge states are associated with the nonzero Chern number. Thus, this topological semimetal shares several properties with the Haldane model but there are also several differences. First, in the momentum space there appears only a Dirac-like point. This property is due to the presence of a zero-energy flat band for $M = 0$ and is shared with some three-band realizations of Chern insulators, even if in these last cases, the topological phases are obtained only by introducing spin-orbit interactions [11–15]. Second, in the low-energy regime, the corresponding effective kernel Hamiltonian h_{eff} is not defined by any Dirac or Dirac-Weyl Hamiltonian even if there is a single Dirac-like point. This is possible because h_{eff} is a fully relativistic first-order Hamiltonian, given by

$$h_{\mathrm{eff}} = K[\beta^x, \beta^0]\, p_x + K[\beta^y, \beta^0]\, p_y + M\beta^0, \tag{3}$$

where we have fixed $J = -K$. Here the 3×3 β^μ matrices

$$\beta^0 = \begin{pmatrix} 0 & 0 & -1 \\ 0 & 0 & 0 \\ 1 & 0 & 0 \end{pmatrix}, \quad \beta^x = \begin{pmatrix} 0 & 0 & 0 \\ 0 & 0 & i \\ 0 & -i & 0 \end{pmatrix},$$
$$\beta^y = \begin{pmatrix} 0 & -i & 0 \\ i & 0 & 0 \\ 0 & 0 & 0 \end{pmatrix} \tag{4}$$

satisfy the following conditions:

$$\beta^\mu \beta^\nu \beta^\sigma + \beta^\sigma \beta^\nu \beta^\mu = \beta^\mu \eta^{\nu\sigma} + \beta^\sigma \eta^{\nu\mu}, \tag{5}$$

where $\eta^{\mu\nu}$ is the the relativistic Minkowski metric such that diag $\eta^{\mu\nu} = (-1,1,1)$. The above relations identify a generalized Clifford algebra, called the Duffin-Kemmer-Petiau (DKP) algebra [8]. This algebra is associated with the DKP theory that describes relativistic spin-0 and spin-1 particles by employing the same formalism used by Dirac for spin-1/2 particles. In particular, the effective Hamiltonian in (3) formally describes spin-0 quasiparticles in two dimensions and the corresponding spinor field satisfies the Klein-Gordon equations. Moreover, we remark the fact that the DKP algebra is very different with respect to the angular momentum algebra employed in [11,15]. In the latter case, the effective Hamiltonians describe spin-1 quasiparticles and a masslike term is necessary to achieve gapped Chern phases, while there are no gapless ones. Importantly, the representation of DKP algebra exists in every dimension and this allows us to build higher-dimensional generalizations of the two-dimensional Chern semimetallic phases as will be shown in a future work.

III. EDGE STATES AND ENTANGLEMENT SPECTRUM

As is well known, one of the main properties of topological phases concerns the existence of robust edge states. In particular, in two-dimensional time-reversal broken phases, the number of chiral edge modes coincides with the value of the Chern number. This is well established when the systems have a gapped bulk but still an open question for Chern semimetals. In order to show the edge state energy dispersion we impose open boundary conditions in the y direction and periodic in the x direction. We perform a Fourier transformation that decomposes our two-dimensional Hamiltonian into decoupled one-dimensional Hamiltonians describing chains of length L_y parametrized by p_x. In Fig. 3 it is clear that edge states appear and cross between bands with nontrivial Chern numbers of opposite sign. Here we show that Chern semimetals have topologically protected edge modes by employing the entanglement spectrum [18]. Let us briefly summarize the main properties of the entanglement spectrum for free-fermion systems. First of all, we divide our model, which is placed on a cylinder, in two nonoverlapping subregions through a cut that runs along x, the periodic dimension [19]. The reduced density matrix of the ground state $\hat{\rho}$ of the subsystem is related to the entanglement Hamiltonian $\hat{H}$, i.e., $\hat{\rho} = e^{-\hat{H}}$, and the corresponding eigenvalues ξ_i contain the main information about topological phases. However, in the case of free-fermion Hamiltonians, it is possible to prove that ξ_i are in one-to-one correspondence with the eigenvalues

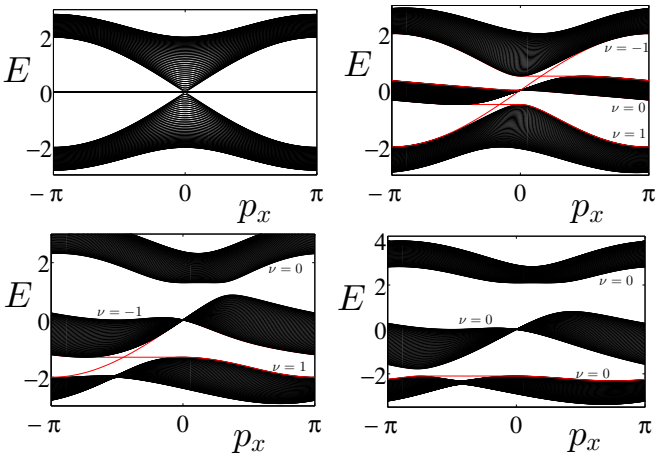

FIG. 3. (Color online) Energy bands for $K = -J = 1$ on cylinder of length $L_y = 80$ as a function of momentum p_x. (Top left) $M = 0$. A single Dirac-like cone and a zero-flat band appear in the system. (Top right) $m = 0.5$ and $\theta = \pi/2$. Upper and lower bands have nonzero Chern number and the crossing red lines represent the edge modes between them. (Bottom left) $m = 1.3$ and $\theta = \pi/4$. The upper gap opens and the Chern number is acquired by the middle band after a topological phase transition when the bands touch. (Bottom right) When even the lower gap opens, the system becomes a trivial insulator.

λ_i of the correlation matrix [20]

$$C_{nm} = \mathrm{tr}(\hat{\rho}\, h_n^\dagger h_m) = \langle gs|h_n^\dagger h_m|gs\rangle, \tag{6}$$

where $|gs\rangle$ is the ground state, the labels m,n are restricted to be within the subsystem, and in our case, h_n represent the fermion operators a_n, b_n, and c_n. Thus, the entanglement spectrum in the model is the spectrum of the correlation matrix. Since our cut runs along the periodic direction x we plot the eigenvalues $\lambda(p_x)$ of the correlation matrix $C(p_x)$ of each of the decoupled chains as shown in Fig. 4, where the ground state used to construct the correlation matrix is built by filling the lower band, and the entanglement cut is placed in the middle of each chain. In this figure the virtual mode in the entanglement spectrum in the plot on the left represented by a gap-crossing line is the signature of the presence of a physical dispersing edge mode that will appear in the energy spectrum when a physical boundary is introduced in the place of the entanglement cut. This edge state is associated with the completely filled lower

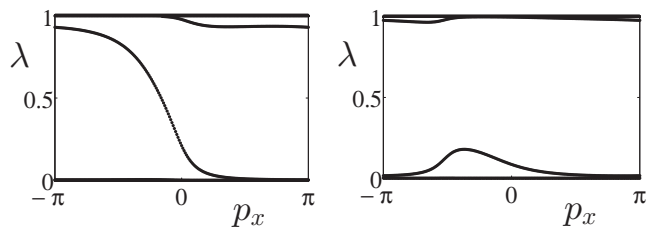

FIG. 4. (Left) The gap-crossing line for $K = -J = 1$, $m = 0.5$, and $\theta = \pi/2$ shows the presence of an edge mode in the entanglement spectrum on the cylinder that represents the signature of the physical edge state. (Right) The absence of the crossing line for $K = -J = 1$, $m \gg 1$, and $\theta = \pi/2$ is due to the absence of edge states in the topologically trivial insulating phase.

band which shows $\nu = 1$. Instead, on the plot on the right, clearly the gap-crossing line disappears in the topologically trivial insulating phase when the band has $\nu = 0$.

IV. DISORDER

In this section we show that the Chern semimetals are even robust phases in the presence of disorder, which would at least weakly appear in the case of experimentally realizing the model with cold atoms in an optical lattice. We impose periodic boundary conditions and divide the systems into four regions: three nonoverlapping regions X,Y,Z with common boundaries that form a triple point which are all surrounded by the fourth region. We then numerically calculate the Chern number in real space [21,22]

$$\nu = 12\pi i \sum_{j\in X}\sum_{k\in Y}\sum_{l\in Z}(C_{jk}C_{kl}C_{lj} - C_{jl}C_{lk}C_{kj}), \qquad (7)$$

which gives the same value as Eq. (2) in the translationally invariant case. Numerically we are restricted to finite system sizes. However, we use system-size scaling in order to see that the real space Chern number converges to an integer as the system size is increased and thus choose an acceptable system size in order to perform our computation. Disorder is introduced in all of the hopping amplitudes $T = K,J,m$ in the form $T(1 \pm J_d)$, where J_d is the disorder amplitude. For each value of J_d we compute the Chern number for a number of disorder realizations and average ν over them. The result as a function of θ and J_d is shown in Fig. 5 (top).

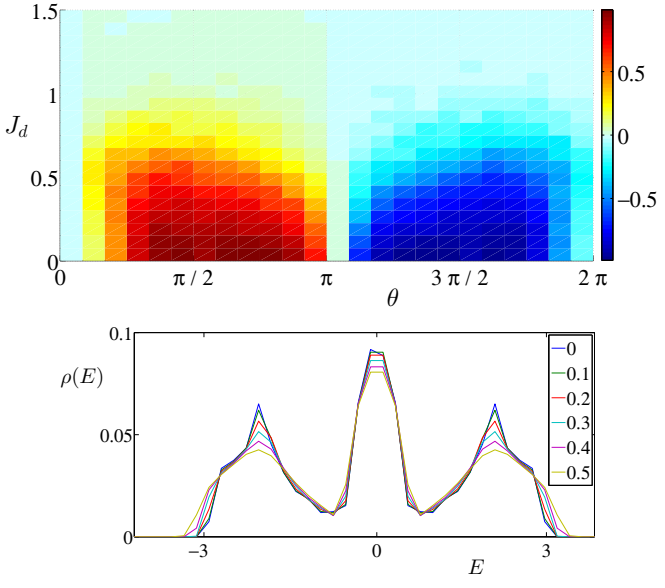

FIG. 5. (Color online) (Top) Real space Chern number ν against θ and J_d for $K = -J = 1$ and $m = 0.5$. Here a system size of 20×20 unit cells is chosen and the particle filling is what corresponds to filling the lowest band in the clean case. Each disorder realization was averaged 20 times, enough to discern the topological regions from the trivial ones. For weak disorder $J_d < 0.5$ the topological phase is robust and for strong disorder the Chern number vanishes. (Bottom) Density of states $\rho(E)$ for disorder amplitudes $0 < J_d < 0.5$ (inset) where we averaged 10^3 disorder realizations on 26×26 unit cells for each J_d. The two minima correspond to the zero indirect gap. The density of states profile does not change around the zero indirect gaps. Here $K = -J = 1$, $m = 0.5$, and $\theta = \pi/2$.

For weak disorder, $J_d < 1$ the topological phase is robust showing a nontrivial value of the Chern number. Since there is no energy gap in the semimetallic phase, we look at the density of states in order to identify the zero indirect gaps, where we have averaged a number of disorder realizations for each disorder amplitude Fig. 5 (bottom). In the clean case the density of states shows minima at the energies where the zero indirect gaps are located. The minima remain for weak disorder and we only notice a spread in the extreme energies away from the zero indirect gaps. This behavior agrees with the Chern number remaining $|\nu| \approx 1$ for weak disorder showing the robustness of the Chern semimetallic phase. It can be shown that the robustness of our model against disorder is comparable to that one of the Haldane model.

V. CONCLUSIONS

Summarizing, we have shown that a simple tight-binding model on the Lieb lattice with only intra-unit-cell and nearest-neighbor hopping terms supports Chern semimetallic phases. These topological semimetals are characterized by a nonzero Chern number in the bulk and topologically protected gapless edge states. We have proved the existence of the latter by studying the entanglement spectrum on the cylinder. Moreover, we have shown that the Chern semimetal is robust also in the presence of weak disorder by calculating the Chern number in the real space. Finally, for its simplicity, our Lieb lattice model can be experimentally realized with cold atoms in an optical lattice [14,23].

ACKNOWLEDGMENT

We thank Jiannis K. Pachos and Chris N. Self for discussions and comments. We are supported by EPSRC Grant No. EP/I038683/1.

APPENDIX

In this Appendix we analyze the semimetal behavior of our system in terms of phase transitions. In order to simplify the calculations but without losing generality, we fix $K = -J = 1$ and $\theta = \pi/2$ in our original tight-binding model, as shown in Fig. 1. In this way, the kernel Hamiltonian h in the momentum space is written as follows:

$$h = \begin{pmatrix} 0 & e^{-ip_x} - 1 & -im \\ e^{ip_x} - 1 & 0 & e^{-ip_y} - 1 \\ im & e^{ip_y} - 1 & 0 \end{pmatrix}. \qquad (A1)$$

First, because the Hamiltonian is traceless, its three eigenvalues $E_1(p_x,p_y,m)$, $E_2(p_x,p_y,m)$, and $E_3(p_x,p_y,m)$ satisfy the following conditions:

$$E_1(p_x,p_y,m) + E_2(p_x,p_y,m) + E_3(p_x,p_y,m) = 0. \quad (A2)$$

Because only two bands are independent, below we are going to analyze only the higher and middle bands, i.e., E_1 and E_2.

Second, we notice that the extrema of the higher and middle bands occur on momenta that live on the diagonal of the Brillouin zone. This implies that we can set $p_x = p_y$ in our

calculations of the extrema. In particular, the minimum of the higher band $E_1^{\min}$ is unique and located at $p_x = 0$ for any value of $m < m_c$. At the same time, the maximum of middle band $E_2^{\max}$ is located at $p_x \approx 1.583$ for any value of $m \leqslant m_c$, see Fig. 6. We determine the value of the critical m numerically to be $m_c \approx 1.4$ as shown in Fig. 6.

When a phase transition occurs for $m = m_c$, the bands touch each other. In this critical case, $E_1^{\min}$ becomes doubly degenerate, i.e., at another momentum $p_x \approx 1.583$ the higher band comes down to the same value as the value it has for $p_x = 0$. The value of the minimum of the higher band which coincides with the maximum of the middle band is a function of m for $m \leqslant m_c$, given by

$$E_1^{\min} = E_2^{\max} = \sqrt{\frac{3}{2}}\, m. \tag{A3}$$

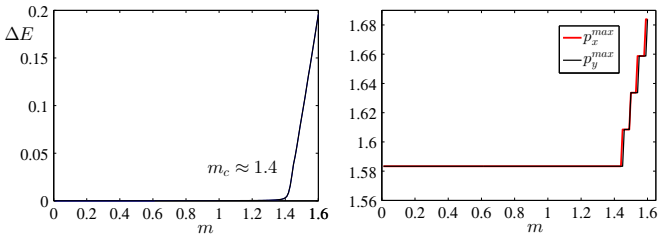

FIG. 6. (Color online) Left: Opening of the indirect gap $\Delta E = E_1 - E_2$ of the model when m_c is reached. Right: The momentum $p_x^{\max}, p_y^{\max}$ where the maximum of the middle band occurs. As the parameter m is varied and as long as $m \leqslant m_c$, the position of the maximum does not move. The lines are degenerate because the extrema of the bands occur on the diagonal of the Brillouin zone.

[1] A. P. Schnyder, S. Ryu, A. Furusaki, and A. W. W. Ludwig, Phys. Rev. B **78**, 195125 (2008).
[2] F. D. M. Haldane, Phys. Rev. Lett. **61**, 2015 (1988).
[3] N. Read and D. Green, Phys. Rev. B **61**, 10267 (2000).
[4] A. A. Burkov and L. Balents, Phys. Rev. Lett. **107**, 127205 (2011).
[5] S. M. Young, S. Zaheer, J. C. Y. Teo, C. L. Kane, E. J. Mele, and A. M. Rappe, Phys. Rev. Lett. **108**, 140405 (2012).
[6] N. Goldman, E. Anisimovas, F. Gerbier, P. Ohberg, I. B. Spielman, and G. Juzeliūnas, New J. Phys. **15**, 013025 (2013).
[7] T. Andrijauskas, E. Anisimovas, M. Račiūnas, A. Mekys, V. Kudriašov, I. B. Spielman, and G. Juzeliūnas, Phys. Rev. A **92**, 033617 (2015).
[8] R. A. Krajcik and M. M. Nieto, Phys. Rev. D **10**, 4049 (1974).
[9] S. Matsuura, P.-Y. Chang, A. P. Schnyder, and S. Ryu, New J. Phys. **15**, 065001 (2013).
[10] E. Dagotto, E. Fradkin, and A. Moreo, Phys. Lett. B **172**, 383 (1986).
[11] D. Green, L. Santos, and C. Chamon, Phys. Rev. B **82**, 075104 (2010).
[12] C. Weeks and M. Franz, Phys. Rev. B **82**, 085310 (2010).
[13] W.-F. Tsai, C. Fang, H. Yao, and J.-P. Hu, New J. Phys. **17**, 055016 (2015).
[14] N. Goldman, D. F. Urban, and D. Bercioux, Phys. Rev. A **83**, 063601 (2011).
[15] W. Beugeling, J. C. Everts, and C. Morais Smith, Phys. Rev. B **86**, 195129 (2012).
[16] T. Louvet, P. Delplace, A. A. Fedorenko, and D. Carpentier, Phys. Rev. B **92**, 155116 (2015).
[17] T. Fukui, Y. Hatsugai, and H. Suzuki, J. Phys. Soc. Jpn. **74**, 1674 (2005).
[18] H. Li and F. D. M. Haldane, Phys. Rev. Lett. **101**, 010504 (2008).
[19] M. Hermanns, Y. Salimi, M. Haque, and L. Fritz, J. Stat. Mech. (2014) P10030.
[20] I. Peschel and V. Eisler, J. Phys. A: Math. Theor. **42**, 504003 (2009).
[21] A. Kitaev, Ann. Phys. **321**, 2 (2006).
[22] J. Bellissard, A. van Elst, and H. Schulz-Baldes, J. Math. Phys. **35**, 5373 (1994).
[23] R. Shen, L. B. Shao, B. Wang, and D. Y. Xing, Phys. Rev. B **81**, 041410(R) (2010).